Chapter 5
Electrochemical Tests in Reinforced Mortar Undergoing Stray Current-Induced Corrosion

Zhipei Chen, Dessi A. Koleva, and Klaas van Breugel

Abstract Stray current, arising from direct current electrified traction systems, further circulating in nearby reinforced concrete structures may initiate corrosion or accelerate existing corrosion processes on the steel reinforcement. In some extreme conditions, corrosion of the embedded steel will occur at very early stage. One of the significant consequences is loss of bond strength and premature failure of the steel-matrix interface. This plays an important role for the integrity of a structure during its designed service life.

In this work, the level of stray current was set at 0.3 mA/cm^2, applied as an external DC electrical field. This level of stray current was chosen based on preliminary calculations on expected corrosion damage, i.e., in view of material loss at the level of 10% weight loss of the steel rebar (analytically calculated via Faraday's law). The investigated reinforced mortar specimens were cured for 24 h only and then conditioned in chloride-free and chloride-containing environment. The evolution of steel electrochemical response in rest (no stray current) and under current conditions was monitored for approx. 240 days via OCP (Open Circuit Potential), LPR (Linear Polarization Resistance), EIS (Electrochemical Impedance Spectroscopy) and PDP (Potentio-dynamic Polarization).

The results show that the effect of stray current on concrete bulk matrix properties, together with steel corrosion response, is significantly determined by the external environment, as well as by the level of maturity of the cement-based bulk matrix.

For chloride-free environment the effect of the chosen stray current level was not significant, although lower corrosion resistance of the steel rebars was

Z. Chen (✉) • K. van Breugel
Faculty of Civil Engineering and Geosciences, Department Materials and Environment, Delft University of Technology, Stevinweg 1, 2628, CN, Delft, The Netherlands
e-mail: z.chen-1@tudelft.nl

D.A. Koleva
Delft University of Technology, Faculty of Civil Engineering and Geosciences, Section Materials and Environment, Stevinweg 1, 2628, CN, Delft, The Netherlands

L.E. Rendon Diaz Miron, D.A. Koleva (eds.), *Concrete Durability*,
DOI 10.1007/978-3-319-55463-1_5

recorded after longer exposure of ~240 days, compared to control conditions. In fact, even positive effects of the stray current were observed in the early stages, i.e., until 28 days of age: stray current flow through a fresh (non-mature) cement matrix led to enhanced water and ion transport due to migration. The result was enhanced cement hydration, consequently environment, assisting a more rapid stabilization of pore solution and steel/cement paste interface. In chloride-containing external medium, steel corrosion was a synergetic effect of both de-passivation due to chloride ions in the medium and stray current effects. Corrosion acceleration solely due to the stray current flow in chloride-containing medium cannot be claimed for the chosen current density levels and the duration and conditions of the experiment.

What can be concluded is that the effect of stray current for both chloride-free and chloride-containing conditions is predominantly positive in the initial stages of this test. The expected negative influence towards corrosion acceleration was observed after a prolonged treatment, when a stable maturity level of the cement-based matrix was at hand. This also means that the properties of the cementitious material in reinforced cement-based system are of significant importance and largely determine the electrochemical state of the steel reinforcement.

Keywords Stray current • Steel corrosion • Mortar • Electrochemical tests

5.1 Introduction

In electrical current powered traction systems, such as electrical trains, tram systems or underground trains, the current drawn by the vehicles returns to the traction power substation through the running rails. This concept, besides forming part of the signaling circuit for controlling the train movements, is used as the current return circuit path, together with return conductors [1–5]. However, owing to the longitudinal resistance of the rails and their imperfect insulation to the ground, part of the return current leaks out from the running rails, i.e., stray current forms. The leaking-out stray current returns to the traction power substation through the ground and underground metallic structures (such as steel rebars in concrete, pipelines), as schematically shown in Fig. 5.1 [6, 7]. Stray direct currents (DC) are known to be more dangerous than stray alternating currents (AC) [3, 8, 9]. Such situation can be potentially very harmful for underground reinforced concrete structures for example, where despite the high concrete resistivity the steel reinforcement provides a good conductive path. The circulation or flow of stray current through reinforced concrete structures may initiate corrosion or significantly accelerate already existing corrosion processes on the steel reinforcement [1].

For a reinforced concrete structure, buried near a rail track, a DC stray current leakage will initiate or enhance steel corrosion as follows: at the point where the

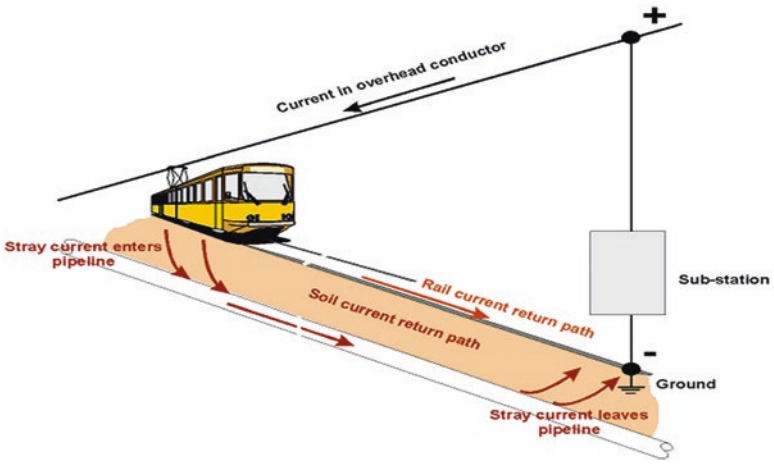

Fig. 5.1 Example of stray current from a railway line picked up by pipeline [10]

stray current "enters" the reinforcement, a cathodic reaction occurs (predominantly oxygen reduction for this environment):

$$\frac{1}{2}O_2 + H_2O + 2e^- \rightarrow 2OH^- \tag{5.1}$$

The point where the stray current flows out from the reinforcement into the external environment (e.g., concrete, soil), anodic reaction occurs which is the process of metal dissolution:

$$Fe \rightarrow Fe^{2+} + 2e^- \tag{5.2}$$

In some extreme conditions (for instance, newly built reinforced concrete structures nearby seaside and/or railways), stray current-induced corrosion of the steel reinforcement could occur at early age and can be significant. This is because of the lower level of maturity of the cement-based matrix in young concrete, which would in turn facilitate the stray current-induced corrosion on the steel surface. Lower electrical resistivity, higher porosity, permeability, diffusivity, etc. of the concrete matrix would lead to enhanced aggressive ions penetration in addition to elevated ion and water migration due to the stray current flow. On the one hand, for a non-matured cement-based matrix and at early stages of cement hydration, elevated ion and water migration can have a positive effect in view of enhanced cement hydration and chloride-binding capacity of the bulk material [11, 12]. However, at later stages and for an already developed bulk matrix microstructure, stray current flow

can affect the pore space and hydration products' network due to leaching-out of calcium baring phases, coarsening of the pore structure, etc. [13]. These will in turn enhance the purely electrochemical reactions, related to the corrosion process on the steel reinforcement. One of the significant consequences is the premature failure of the steel-matrix interface, i.e., significantly reduced bond strength, which plays important role for the integrity of a structure during the subsequent service life. These phenomena lead frequently to early deterioration and eventually to situations of high risk in view of durability and serviceability of reinforced concrete structures. By all means, the above concerns are also linked to high cost for maintenance and repair, targeting safe operation of such structures.

This work aimed to simulate stray current-induced corrosion for reinforced concrete and investigate the electrochemical response of the steel reinforcement in comparison to control (stray current-free) conditions. In order to account for the significant effect of environmental conditions, mainly the presence of chloride ions as a corrosion accelerator, the stray current conditions were simulated in both chloride-free and chloride-containing medium. The level of stray current was set at 0.3 mA/cm^2 (through the application of external DC electrical field). This level of current density was chosen in a way to account for a hypothetic 10% weight loss of the steel rebar.

The overall aim of the research project on stray-current corrosion, this work being an initial part of it, is to correlate the electrochemical response of steel (corrosion state) with bond strength at the steel/cement paste interface and bulk matrix properties. This chapter focuses only on the initial results from electrochemical monitoring of reinforced mortar specimens in the time frame of the test of 243 days. Several types of general and more sophisticated electrochemical tests are presented and discussed in view of the effect of stray current on the corrosion state of steel reinforcement. Additionally, the development and alterations in the properties of the bulk matrix were indirectly evaluated, owing to the possibility of one of the electrochemical non-destructive techniques (i.e., electrochemical impedance spectroscopy) to provide qualitative and quantitative information for both steel- and cement-based material properties.

5.2 Experimental

5.2.1 Materials and Specimen Preparation

Reinforced mortar prisms of 40 mm × 40 mm × 160 mm were cast from Ordinary Portland cement CEM I 42.5 N and normed sand. The water-to-cement (w/c) ratio was 0.5; the cement-to-sand ratio was 1:3. Construction steel (rebar) FeB500HKN (d = 6 mm) with exposed length of 40 mm was centrally embedded in the mortar prisms (Fig. 5.2). Prior to casting, the steel rebars were cleaned electrochemically (cathodic treatment with 100 A/m^2 current density, using stainless steel as anode) in

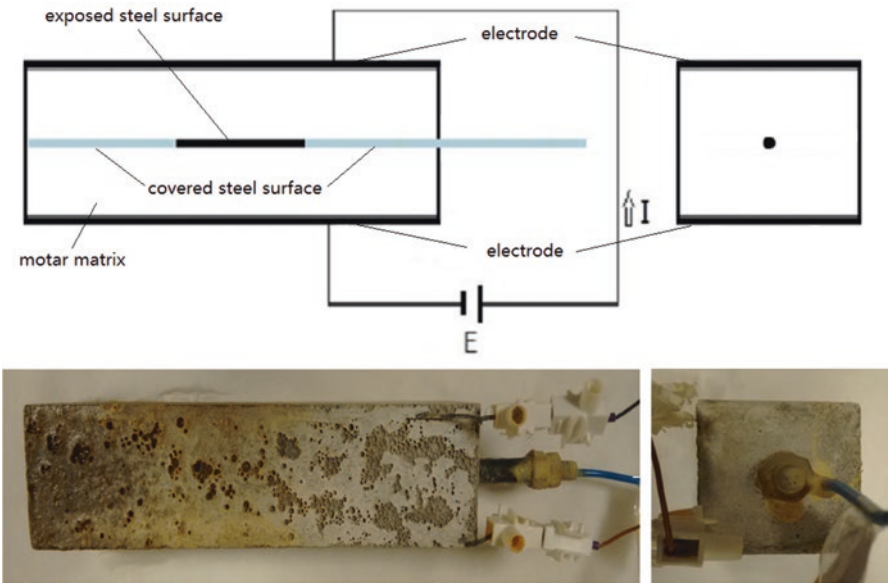

Fig. 5.2 Experimental setup and position of electrodes for stray current supply

a solution of 75 g NaOH, 25 g Na_2SO_4, 75 g Na_2CO_3, reagent water to 1000 mL, according to ASTM G-1 [14, 15]. The schematic presentation of the specimens' geometry is depicted in Fig. 5.2: the two ends of the rebars were covered by heat-shrinkable tube, in order to restrict the exposed surface area.

The experimental setup and electrodes' configuration for supplying stray current (with the level of 0.3 mA/cm^2) are as presented in Fig. 5.2: two Ti electrodes (MMO Ti mesh, 40 mm × 160 mm) cast-in within samples preparation served as terminals for stray current application. When the stray current supply was interrupted (min 24 h before electrochemical tests), the Ti electrodes served as counter electrode in a general 3-electrode setup, where the rebar was the working electrode and an external SCE (Saturated Calomel Electrode) served as a reference electrode.

5.2.2 Curing Conditions

After casting and prior to demoulding and conditioning, all specimens were cured in a fog room (98% RH, 20 °C) for 24 h. The specimens were lab conditioned after demoulding. All specimens were immersed with two-third of height in water or 5% NaCl solution. Table 5.1 summarizes the relevant conditions and specimens' designation.

Table 5.1 Details of conditioning regimes

Group	External environment	Current supply
R	Water (2/3)	–
C	5% NaCl (2/3)	–
S	Water (2/3)	Stray current
CS	5% NaCl (2/3)	Stray current

5.2.3 Level of Stray Current Regime: Considerations

Besides present work, a series of side-by-side tests have also been performed to compare the effects of stray current and direct anodic polarization on the corrosion behavior of steel embedded in mortar specimens, due to the fact that some current state-of-the-art generally reports on simulating stray current corrosion through anodic polarization.

For a hypothetic 10% weight loss of the steel rebar reduced by anodic polarization, the applied current density (i.e., level of anodic polarization) can be expressed as a function of duration of the corrosion process and predefined corrosion degree as follows, based on Faraday's law:

$$i = \frac{ZFr\rho\eta_s}{2At} \tag{5.3}$$

where t is time of corrosion (for the feasibility of calculation, the duration of 28 days has been chosen preliminarily, 28 days =2,419,200 s), Z is the valence of the metal ions taking part in the anodic reaction, which is 2 in this case (iron), F is Faraday's constant (F = 96,500 As), r is the radius of corroded bar (0.3 cm), $\rho$is the density of iron (ρ= 7.87 g/cm^3), $\eta_s$is the mass loss ratio (10%), A is the atomic mass of iron (A = 56 g) and i is the impressed current density (A/cm^2).

Based on the calculation, the level of anodic polarization corresponding to 10% mass loss is 0.1744 mA/cm^2. Considering the fact that the supplied anodic current may not all take part in the oxidation of iron in mortar matrix, part of it may be involved in other reactions. So for this consideration, the final chosen current level was increased and set at 0.3 mA/cm^2.

For the convenience of comparison between stray current and anodic polarization, levels of stray current and anodic polarization are both set at 0.3 mA/cm^2.

5.2.4 Testing Methods

The electrochemical measurements were performed at open circuit potential (OCP) for all specimens, using SCE as reference electrode (as above specified, the counter electrode was the initially embedded MMO Ti). The used equipment was Metrohm Autolab (Potentiostat PGSTAT302N), combined with a FRA2 module.

Electrochemical impedance spectroscopy (EIS) was employed in the frequency range of 50 kHz − 10 mHz, by superimposing an AC voltage of 10 mV (rms). Linear polarization resistance (LPR) was performed in the range of ±20 mV vs OCP, at a scan rate of 0.1 mV/s. Both EIS and LPR tests were performed after 3, 7, 14, 28, 56, 141, 215 and 243 days of conditioning. Prior to each EIS and LPR test, a 24 h depolarization (potential decay) was recorded to assure stable OCP after stray current interruption. During the depolarization process and within electrochemical tests, the specimens were immersed fully in the relevant medium. The control samples (Group R) were also monitored according to the above test procedure. At the end of conditioning (at the age of 243 days), PDP (potentio-dynamic polarization) was performed in the range of −0.15 V to +0.90 V vs OCP at a scan rate of 0.5 mV/s, in order to additionally collect information for the electrochemical state of the steel reinforcement.

5.3 Results and Discussion

The outcomes from electrochemical tests are presented and discussed starting from non-destructive tests – e.g., OCP records and EIS measurements throughout the experiment, followed by results from polarizations tests (PDP) at the end of the test. A relatively larger portion of the below discussion is on OCP records in view of considerations for the expected and unexpected electrochemical response of the embedded steel in this work. EIS results are mainly discussed as a qualitative assessment in view of bulk matrix properties and steel surface active/passive state, however, also including a global quantitative assessment of corrosion state over time. Finally, the PDP tests support the results and discussion in the preceding OCP and EIS sections.

5.3.1 Open Circuit Potentials and Polarization Resistance

5.3.1.1 General Considerations OCP Readings and R_p Values

The general meaning of OCP values and their evolution in time accounts for the global corrosion state of the steel reinforcement – active or passive. Figure 5.3a also indicates the threshold for passive to active state for steel in cement-based materials, as defined by accepted standards and criteria [10]. The OCP values are used for a qualitative assessment only of corrosion state. In contrast, R_p values are used for a quantitative assessment, through calculating corrosion current by employing the Stern-Geary equation, i.e., $i_{corr} = B/R_p$ [16]. The R_p value is experimentally derived, whereas the constant B can be either experimentally derived or reported values for passive (B = 52 mV/dec) or active (B = 26 mV/dec) state can be employed [16]. Since R_p is inversely proportional to the corrosion current, quantification of

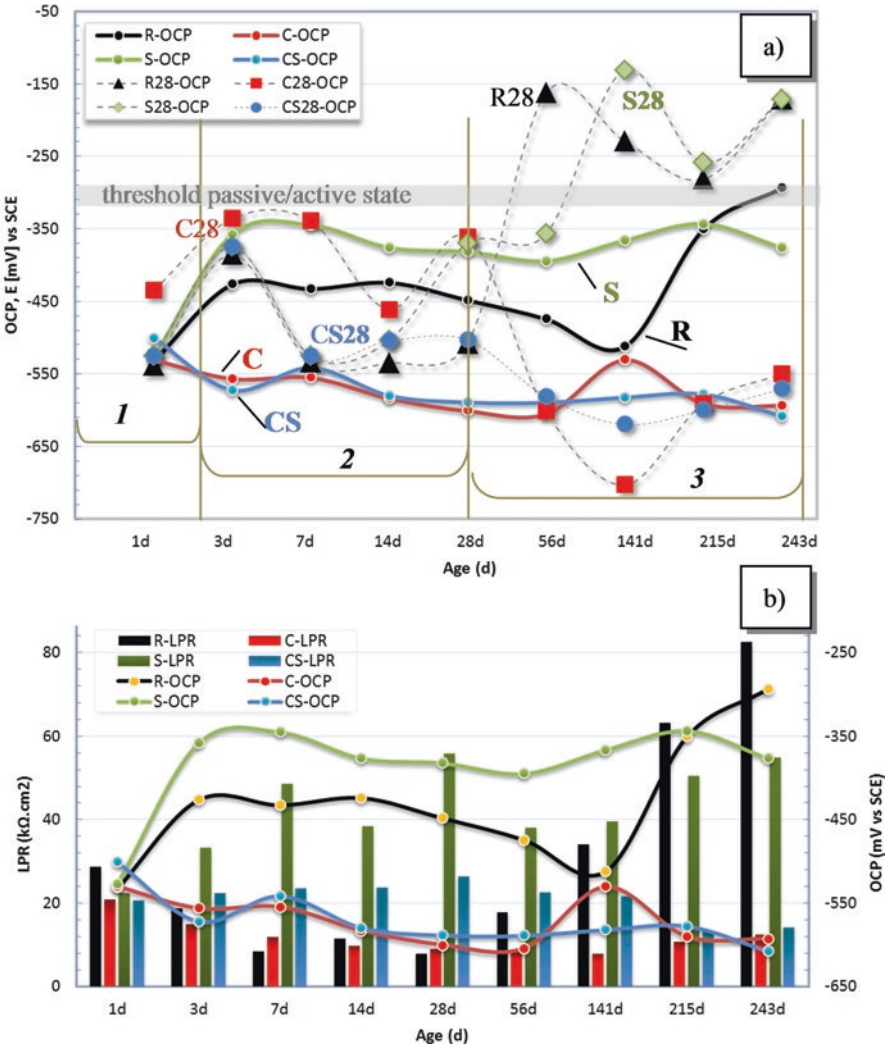

Fig. 5.3 (**a**) OCP evolution with time (1 –243 days) for specimen groups: *R* Reference, *C* corroding (NaCl medium), *S* Stray Current, *CS* Corroding (NaCl) + Stray Current – all after *24 h curing* and subsequently conditioned until 243 days; (**b**) evolution of R_p values and correlation to OCP values over time for specimen groups *R, C, S* and *CS*. For comparative purposes, Fig. 5.3**a** also depicts the OCP evolution for *R, C, S* and *CS* specimens from parallel groups, cured *for 28 days* with designation R28, C28, S28 and CS28

corrosion resistance can be performed by a comparative analysis of R_p values only, as used and discussed in this work.

Figure 5.3a depicts the evolution of open circuit potentials (OCP), Fig. 5.3b presents the evolution of polarization resistance (R_p) values as recorded via LPR measurements, together with the OCP records. Figure 5.3a depicts the OCP evolution

for the discussed in this paper series of specimens, cured for 24 h only ("24-hour" groups R, C, S and CS).

The OCP values, recorded for identical, but cured for 28 days specimen groups ("28-day" groups R28, C28, S28 and CS28) are also presented for comparative purposes. The 28-day cured specimens are not subject to this work. However, in order to elucidate the initial electrochemical state in terms of OCP records, and mainly to clarify discrepancies between observed and generally expected response, the 28-day series is briefly discussed with this regard. To be noted is that the OCP values for the 28-day series were recorded also during curing of 1–28 days, when no further conditioning or external factors applied. The OCP values for groups S and CS (stray current involved), in both 24-h and 28-day cured groups, were recorded after current interruption and 24 h decay respectively.

5.3.1.2 OCP Values and Curing Age

In this study, except the conditioning regimes and relevant environment, factors as steel pre-treatment, mortar curing and the additional variable "stray current" are determining the electrochemical response and OCP development, respectively. As can be observed in Fig. 5.3a, the majority of OCP values for the 24-h cured specimens R, C, S and CS until the 28 days of age and beyond fall in the cathodic region and were more negative than the threshold of passivity, i.e., more cathodic than the generally accepted -200 ± 70 mV vs SCE for reinforced mortar (concrete) systems [15]. These OCP values account for active state of the steel reinforcement in all conditions, including the control R group, for at least until 28 days of age. Except the conditioning regimes and external influences (as stray current) there are three main reasons/factors for the observed behavior:

(i) The steel surface properties prior to casting
(ii) The maturity of the cement-based matrix, which determines the pH of the pore solution
(iii) The porosity/permeability of the mortar bulk determining chloride ions penetration in corroding conditions, as well as water penetration and oxygen levels in all conditions

The first factor (steel surface properties) will affect both 24-h and 28-days cured groups. This aspect is of importance in the sense that clean steel surface would be relatively more active compared to oxide layer-covered ("as received") steel, until a stable passive layer is formed in the high pH environment of the mortar pore network. The pH of the pore solution is initially >13.5 in the first hours of cement hydration and stabilizes further to approx. pH of 12.9. In a medium of pH > 13.5 steel is active, following fundamental electrochemical thermodynamics.

The second and third factors, related to cement-based material properties, would predominantly affect the response in the 24-h cured group, whereas different behavior would be expected in the 28-days cured group. This is denoted to a "fresh" state in the former case (only 24 h curing) and higher maturity level in the latter case (the

generally employed in cement-based material science 28-day curing). On the other hand, this means that for the period of 1d to 28 days of monitoring, both 24-h and 28-days cured specimen groups should exhibit similar OCP records. However, variation in OCP for the 24-h cured groups will be additionally present as a result from the conditioning regimes in that period. In contrast, the OCP records for the 28-day cured specimens in the same time interval will represent the steel response within cement hydration only.

To this end, Fig. 5.3a can be considered as presenting three main regions of OCP evolution: initial response – *region 1* and day 1, followed by 3–28 days of conditioning – *region 2*, and beyond 28 days to final response at the end of the test for the 24-h cured group – *region 3* (the tests for the 28-day cured series of specimens is ongoing).

5.3.1.3 OCP Evolution Until 28 Days of Age

For all specimens and irrelevant of the curing period (i.e., both 24-h and 28-day cured groups), the initial readings in *region 1*, Fig. 5.3a depict cathodic OCP values in the range of −550 mV to −420 mV, which are far beyond the passivity threshold. This is as expected due to the surface condition of the embedded steel (clean surface), the fresh mortar matrix and related phenomena within cement hydration and pH of the pore solution, as previously discussed. In other words, the electrochemical cleaning of the embedded steel, performed prior to casting, results in a "bare" steel surface, which will be active in alkaline environment of pH > 13.5 until a passive layer is formed and the pH of the environment stabilizes around 12.9.

In *region 2*, Fig. 5.3a, i.e., 3 days until 28 days period for the 24-h cured groups (within conditioning) and the 28-day cured groups (curing only), the OCP records reflect the steel electrochemical response within pore network and steel/cement pate interface development. These are in terms of pore solution chemistry alterations as well as passive layer stabilization (for control cases) or corrosion initiation (for corroding cases). The development of the passive layer and further stabilization is illustrated by the initial fluctuations of OCP values for the control groups R and R28 and stabilization further on, towards more anodic values. For the 28 day-cured control specimens (R28 in Fig. 5.3a), OCP values in the passive domain only were recorded after 28 days of age. In contrast, stabilization of the passive layer for specimens R in the 24-h cured group takes significantly longer period – after 141 days of conditioning, OCPs start tending towards more anodic values. In the former case (28-days group), this development is as expected and already discussed. For the latter case, 24 h curing leads to an open microstructure, non-mature matrix and consequently altered balance of pore water and alkali ions concentration in the pore network. This results in impeding the passive layer formation and development for the control group R, although OCP values are more anodic than these for the corroding groups C and CS between 3 and 28 days of conditioning. For the C and CS groups, active steel surface is expected due to chloride-induced corrosion initiation in both cases and additional stray current contribution in the case of CS specimens.

A pronounced effect of the stray current in group CS towards enhanced corrosion was, however, not observed through OCP records: as shown in Fig. 5.3a, the OCP evolution for specimens C and CS follows similar development over time.

What should be noted is that the stray current in control conditions – group S, was expected to have a negative effect on steel corrosion resistance. This, however, was not observed. On the contrary, the recorded OCP values in *region 2* for specimens S are more anodic than those for specimens R and maintain stability also within region 3. This observation is, however, only relevant for group S which are specimens cured for 24 h only, but is not relevant for groups S28, cured for 28 days. The related phenomena are as follows: for group S, stray current flow through a fresh (non-mature) cement matrix will lead to enhanced water and ion transport due to migration. As a result, cement hydration will be enhanced, leading to a faster development of the pore network and consequently environment, assisting a more rapid stabilization of pore solution and steel/cement paste interface. Previously reported and known are the early stage beneficial effects of stray current on cement-based matrix properties [13].

To this end and with relevance to *region 2* in Fig. 5.3a, the specimens S end up with a superior corrosion resistance, compared to the control specimens R, when 24 h curing only is relevant. In contrast, the stray current applied to group S28 was only after 28 days of curing. Consequently, within *region 2* (3 days until 28 days) the OCP evolution for both R28 and S28 groups is similar, since all specimens in the 28-days cured group can be considered as control, i.e., there are no external factors involved, but only cement hydration is taking place. Therefore, the OCP records for groups R28, C28, CS28 and S28 present similar, although fluctuating, OCP records in ***region 2***, which are in the range of these recorded for control specimens R and the specimens S (stray current flow in water environment) from the 24-h cured groups.

5.3.1.4 OCP Records from 28 Days of Age Until the End of the Test (243 days) and R_p Evolution for the 24-h Cured Specimens

A more pronounced differentiation between the 24-h and 28-day cured specimens in electrochemical response, due to environmental effects, stray current and variation of bulk matrix properties, can be already observed in *region 3*, Fig. 5.3a, i.e., from 28 to 243 days. It should be noted that for specimens R28, C28, S28 and CS28, the 28 days' time interval actually corresponds to 28 days of age but 1 day of conditioning only, whereas for specimens R, C, S and CS, the 28 days' time interval corresponds to 28 days of age and 28 days of conditioning. Relevant to ***region 3***, time interval of 56 days, it can be observed that for the corroding groups, where NaCl is present in the environment (C, CS, C28 and CS28), all OCP values fall within similar range of values, more cathodic than −550 mV, reflecting active state. Similar to *region 2*, a pronounced effect of the stray current (groups CS) was not distinguished through OCP records, if these are compared to values for specimens C. For the control groups – R and R28, passive layer stabilization and transition

from “active” to “passive” domain was observed, especially for group R towards the end of the test. Similarly, the R28 group presents OCP values in the region of passivity, i.e., in the range of −250 mV to −150 mV.

For the 28-day cured groups under stray current, the S28 specimens depict OCPs similar to those for group R28. Apparently, a negative effect of stray current on the corrosion resistance of the embedded steel, especially when applied after 28 days of curing (as is the case for group S28) is not to be observed via OCP records for the relevant time span of this test.

In contrast, for group S, where the stray current application was initiated after 24-h curing only, the initially stable and more anodic values in *region 2* tend to shift to values which are already more cathodic than these for specimens R in the same 24-h cured groups. The OCP development for group S exhibits a stabilization trend below the threshold for active/passive state and remains in the active region. In other words, further records (after 243 days) would possibly reflect already the expected negative effect of stray current on steel corrosion resistance. This hypothesis is supported by the derived R_p values, where a trend towards lower R_p, i.e., lower corrosion resistance, was observed for specimens S, compared to specimens R after prolonged conditioning (Fig. 5.3b). After initially highest R_p values, the corrosion resistance for specimens S was reduced, which is in contrast with the trend of R_p increase for specimens R towards the end of the test.

The R_p values for the corroding, NaCl conditioned, groups C and CS maintain low R_p values throughout the reported period. Lower R_p values were recorded for specimens C if compared to those for specimens CS. However, towards the end of the test the corrosion activity for C and CS is almost equally high. This observation reflects the previously discussed hypothesis for the expected negative effect of stray current in specimens CS only with prolonged conditioning. Obviously, competitive mechanisms act in specimens CS, where on the one hand the stray current has positive effects on bulk matrix properties, similar to specimen S, at early stages. On the other hand, stray current influences chloride ions migration, leading to chloride-induced corrosion and active state, similarly to specimens C. Here again, a conclusive statement on the effect of stray current on corrosion resistance in both S and CS groups cannot be made, if considerations are based only on OCP and R_p evolution during the reported time interval of this experiment.

5.3.2 EIS and PDP Response

EIS is a non-destructive electrochemical technique, which when applied to a reinforced concrete system provides qualitative and quantitative information for both the electrochemical state of the steel reinforcement and the properties of the bulk matrix. EIS was employed in a manner, similar to previously reported such for an otherwise in-depth characterization of steel-concrete systems [17–19]. The results and discussion in this work refer to time intervals within the period of 243 days of conditioning for all studied specimen groups. Both qualification, by simply

evaluating and comparing EIS response, and quantification of general corrosion state (deriving R_p values) were performed. Absolute values are not claimed but rather a comparison between equally handled specimens is relevant and discussed.

The EIS response was recorded in the frequency range of 50 kHz to 10 mHz. This frequency range provides information for the contribution of the bulk matrix (high frequency (HF) range > 1 kHz) to the electrochemical response of the embedded steel (middle to low frequency ranges, i.e., < 1 kHz and mainly 1 Hz to 10 mHz). Absolute values for concrete bulk properties can be derived at high frequency range, above the 1 MHz region, e.g., starting at 10 MHz [20]. Therefore, the qualification and quantification of the bulk matrix in this work refers to contribution only of the mortar bulk matrix, in terms of: solid phase, connected and disconnected pore network, together with external medium (solution) contribution, which is negligible if compared to that of the bulk matrix.

5.3.2.1 General Considerations Towards EIS Data Interpretation

If a prompt evaluation of the corrosion state of steel embedded in a cement-based material is aimed at, together with a simplified assessment of the electrical properties of the bulk matrix itself, qualification of the EIS response is a very useful approach. This is especially the case if specimens, conditioned in different environment and hence, expected to present significant variation in properties and response, are subject to investigation. For instance, a reinforced mortar specimen conditioned in NaCl will logically perform different in time, if compared to a control specimen conditioned in water. This is due to the expected chloride-induced steel corrosion in the former case and stabilization of the passive state of the steel reinforcement in the latter case.

Additionally, alterations in the electrical properties of the bulk cement-based matrix, e.g., increased electrical resistivity over time, would be expected in all conditions, due to the process of cement hydration and subsequent matrix densification. Similarly, factors as chemical composition of the external environment, ions and water penetration into the bulk matrix, variation in bulk matrix diffusivity, pore interconnectivity, etc. will determine changes in the electrical properties of the bulk matrix over time. These again will be reflected by the EIS response and will vary not only as a result of the corrosion state of the embedded steel but also as a result of conditioning and treatment. All these features in an experimental EIS response are well visible and can be compared qualitatively for systems as in this work – corroding and control reinforced mortar specimens. Additionally, specimens as the hereby discussed “under current regimes” can be indirectly evaluated by a comparison with the corroding and control specimens.

To this end, the EIS response for the hereby studied R, C, S and CS groups of specimens was qualitatively evaluated first. This approach is mainly relevant to the high frequency domain and bulk matrix response, respectively. Next, quantification of the experimental EIS data was performed and the four specimen groups in this

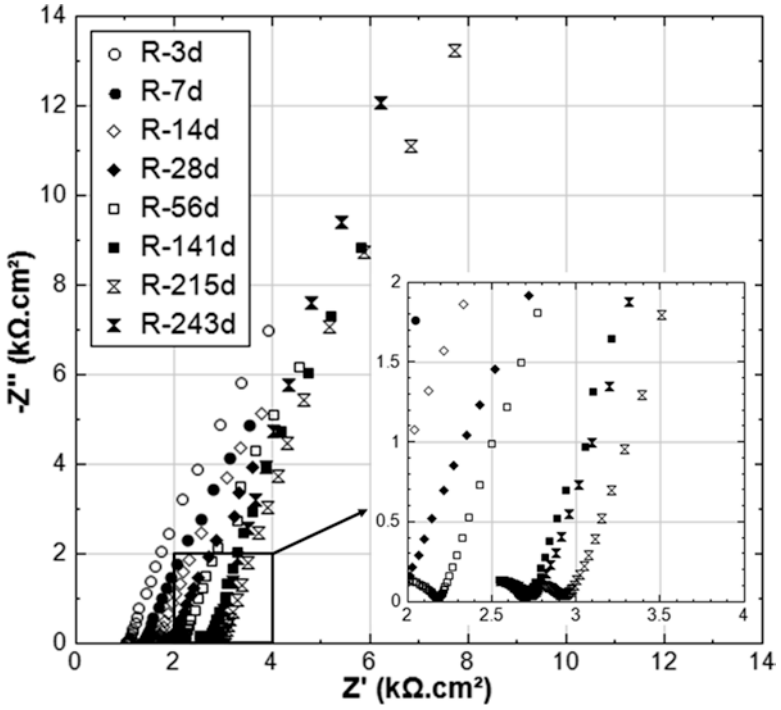

Fig. 5.4 EIS response for Group R as an overlay of 3–243 days

work were compared in view of global corrosion resistance of the embedded steel reinforcement.

The experimental impedance responses, in a Nyquist plot format, for all groups of specimens are presented in Figs. 5.4, 5.5, 5.6 and 5.7 as an overlay from 3 to 243 days per specimens group.

With regard to Group R and S, the shape of the experimental curves in Figs. 5.4 and 5.5 reflects the typical response of steel in a chlorides-free cement-based environment (alkaline medium). The response depicts curves inclined to the imaginary y-axis, reflecting a capacitive-like behavior, or passive state, of the steel reinforcement. This behavior is relevant for group R throughout the test and is more significantly pronounced after 56 days of conditioning, denoted to stabilization of the passive layer over time. The observation is in line with the OCP ennoblement for group R towards the end of the test (Fig. 5.3). For specimens S, although similar to specimens R behavior is relevant at initial time intervals – 3 to 28 days, the magnitude of impedance tends to lower values towards the end of the test, reflected by an inclination of the EIS response towards the real, x-axis. This is also in line with the more cathodic OCP values, recorded for group S towards the end of the test (Fig. 5.3).

In contrast to R and S groups, the EIS responses for groups C and CS, Figs. 5.6 and 5.7, show a clear evidence of active corrosion on the steel surface. Starting at

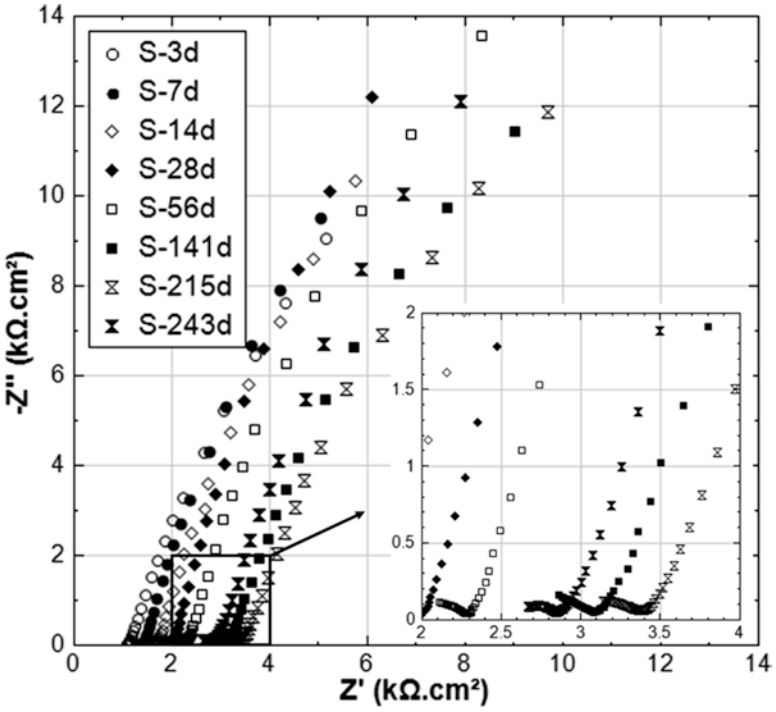

Fig. 5.5 EIS response for Group S as an overlay of 3–243 days

very early stage (3 days) the response is already inclined to the real axis semicircle with a decreasing magnitude of impedance |Z| towards the 243 days. The shape of this EIS response was also largely reported to be due to the presence of chloride ions on the steel surface and increasingly active corrosion state [21].

The Nyquist plots in Figs. 5.4, 5.5, 5.6 and 5.7 also reflect the changes of EIS response in view of bulk matrix characteristics – this is the response in the high frequency domain (inlets in Figs. 5.4, 5.5, 5.6, and 5.7). Additionally and for a more clear comparison in the HF domain, Figs. 5.8 and 5.9 (marked regions) present the EIS response as an overly of magnitude of |Z| in Bode plots format. As previously mentioned, the HF response in this work is with regard contribution only of the bulk matrix, since the measurements were performed, starting from 50 kHz. Therefore a qualitative evaluation and comparison was only made in this frequency domain and is presented in what follows.

5.3.2.2 High Frequency Response and Bulk Matrix Properties

The inlets in Figs. 5.4, 5.5, 5.6 and 5.7 present a more detailed view of the HF response. In other words, the bulk matrix contribution is reflected by the initial, semicircular portion of the EIS experimental curves as depicted in the Nyquist plots.

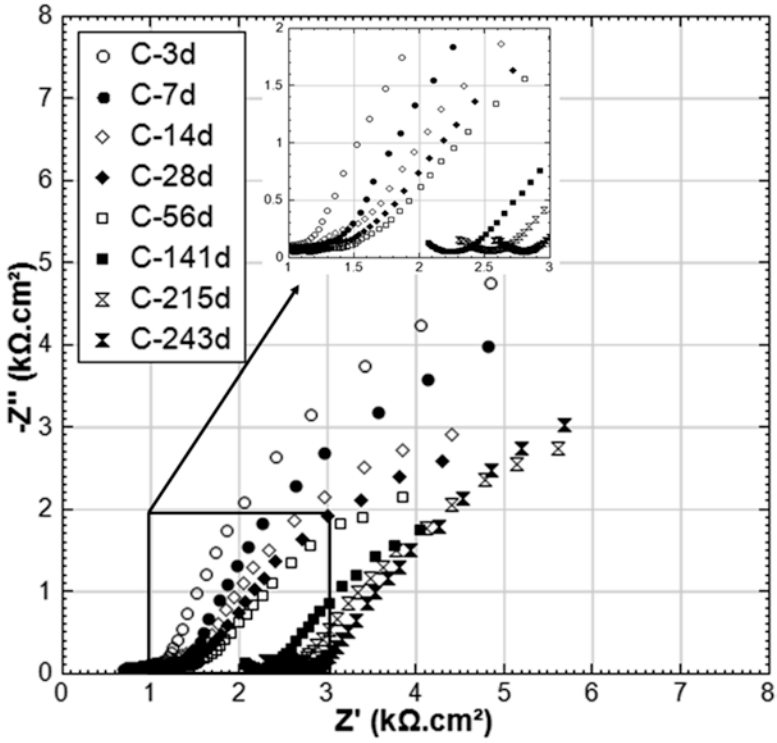

Fig. 5.6 EIS response for Group C as an overlay of 3–243 days

As seen from the plots, an increase in bulk matrix resistance (increase of real |Z| values in the HF domain over time) is relevant for all specimen groups within treatment, irrespective of the external environment. The experimental curves in Figs. 5.4, 5.5, 5.6 and 5.7 are also depicted in a Bode format, Figs. 5.8 and 5.9, presenting log of impedance |Z| vs log frequency. This presentation gives a clearer overview of the changes in the HF domain over time (marked regions in Figs. 5.8 and 5.9), where a trend towards increase of bulk matrix resistance can be observed for all groups.

The HF EIS response, Fig. 5.8, accounts for initially similar properties of the bulk matrix for specimens R and S. Later on and towards the end of the test, bulk matrix densification and/or reduced permeability of the pore network would be relevant for specimens S, evident from increased magnitude of |Z| in the HF domain. The increase of bulk matrix resistance was as expected and due to cement hydration. The result is filling-up of "empty" (pore) space with hydration products, which leads to microstructural development and therefore reduced porosity and permeability. Since cement hydration is affected by water and ions transport/interaction within the pore network, it is also logic that these processes will be enhanced in conditions of current flow, if compared to control conditions. In other words, in addition to diffusion from concentration gradients, ion and water migration take place in specimens

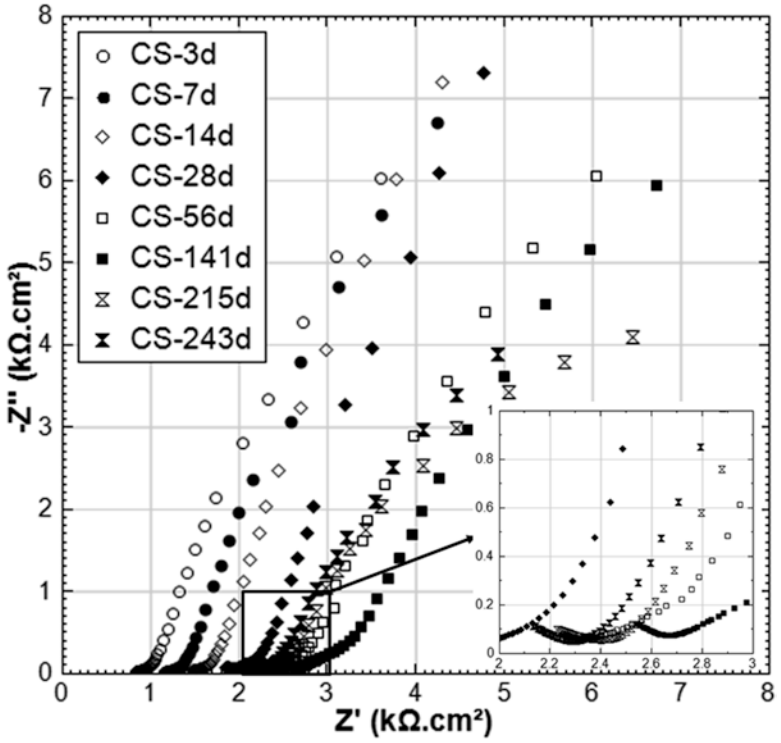

Fig. 5.7 EIS response for Group CS as an overlay of 3–243 days

S, which in turn enhances the related cement hydration mechanisms. The result will be higher bulk matrix resistance as actually recorded by the EIS response, Fig. 5.8.

Different behavior was observed for groups C and CS, additionally related to the chloride ions in the external environment on the one hand (specimens C and CS) and the effect of chloride ions and current flow on the other hand (specimens CS only). Well known is the effect of NaCl on cement hydration. This is in view of acceleration of the hydration process, resulting in matrix densification [22]. This process would be expected to be more pronounced within the additional effect of ions and water migration when current flow is involved, as in CS specimens. The EIS response reflects these changes – Fig. 5.9. The initial HF response for specimens CS showed higher HF impedance values (starting at 3, 7 and 14 days of treatment), compared to that for specimens C at the same time intervals. Later on and towards the end of the test, e.g., 141–243 days, the HF impedance reflecting bulk matrix contribution for both C and CS specimens shows a similar trend and range, Fig. 5.9.

What can be concluded from evaluation and qualitative interpretation of the HF response is that stray current affects the bulk matrix properties. The effect is positive in view of increased bulk matrix resistance and is more pronounced at later stages

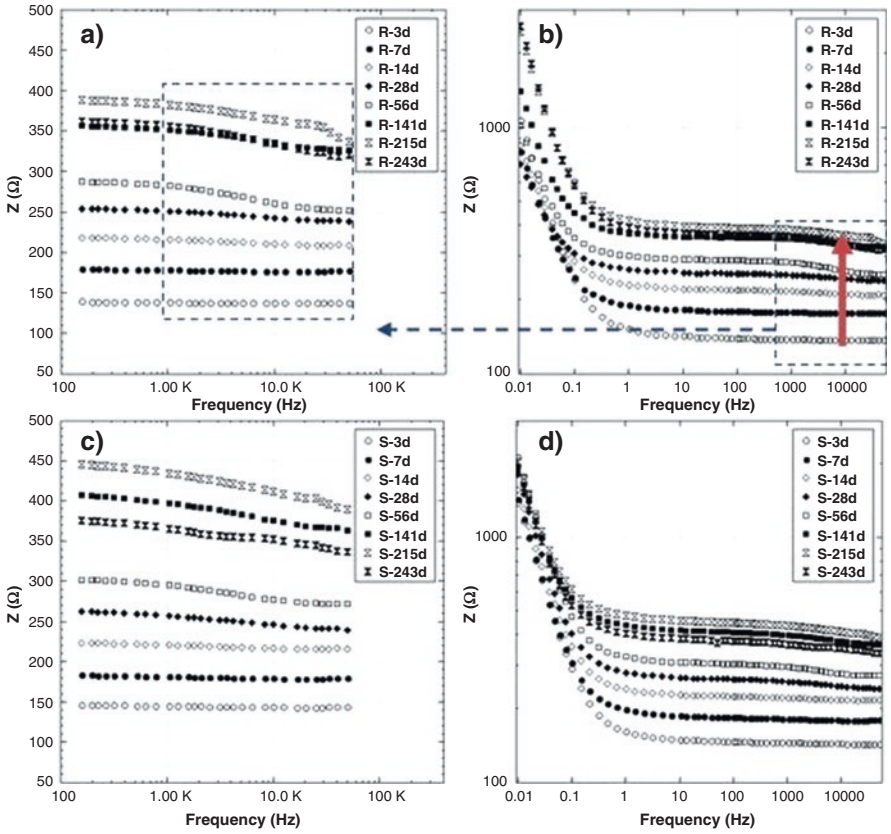

Fig. 5.8 Overlay response from 3 to 243 days for specimens *R* (**a**, **b**) and *S* (**c**, **d**) in Bode plot format – overlay magnitude |Z| in HF-MF domain (50 kHz – 150 Hz)

(after 56 days) for specimens, treated in water (group S compared to group R, Fig. 5.8) and at earlier stages – 3 to 28 days for specimens, conditioned in NaCl (specimens C and CS, Fig. 5.9).

5.3.2.3 Quantification of EIS Response and Global Corrosion State, Including PDP Test

Quantitative information from the EIS response is normally obtained by fitting the experimental data, using the relevant electrochemical software, with an equivalent electrical circuit. The electrical circuit is a sequence of electrical parameters, in series with the electrolyte (external medium) resistance. Each parameter, or a combination thereof, represents a physical meaning, relevant to the EIS response of the system under study. The theory and practice behind EIS response electrochemical

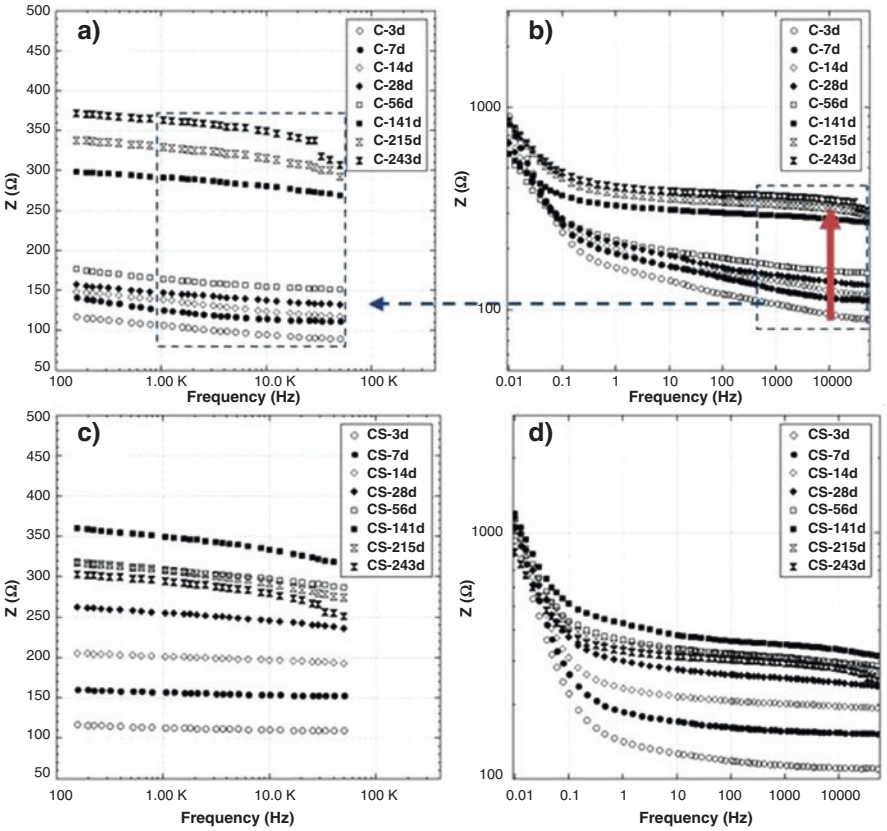

Fig. 5.9 Overlay response from 3 to 243 days for specimens *C* (**a**, **b**) and *CS* (**c**, **d**) in Bode plot format – overlay magnitude |Z| in HF-MF domain (50 kHz – 150 Hz)

fit and simulation, in general or for a reinforced cement-based system, are not subject to this work and can be found in related state of the art [23–25].

An example for experimental response and fit for the studied specimens in this work is presented in Fig. 5.10 in both Nyquist and Bode plots format. The response is not normalized in the examples of Fig. 5.10, since equal geometry of the specimens and steel surface area were relevant for all cases. Figure 5.10a depicts the initial EIS response, after 3 days of treatment, and fit for specimen S. Figure 5.10b depicts the EIS response and fit for a specimen from group CS after 215 days of treatment. Two types of equivalent electrical circuits were used (inlets in Nyquist plots in Fig. 5.10): for the cases of specimens R and S (chloride-free environment) the EIS data were fitted by a circuit with two hierarchical time constants in series with the electrolyte resistance. For the specimens in groups C and CS (chloride-containing external medium), the circuit was composed of three time constant.

For both circuits, R_0 is the electrolyte resistance, together with the contribution of the mortar bulk. In the two-time constant circuit, the first time constant (R_1 and

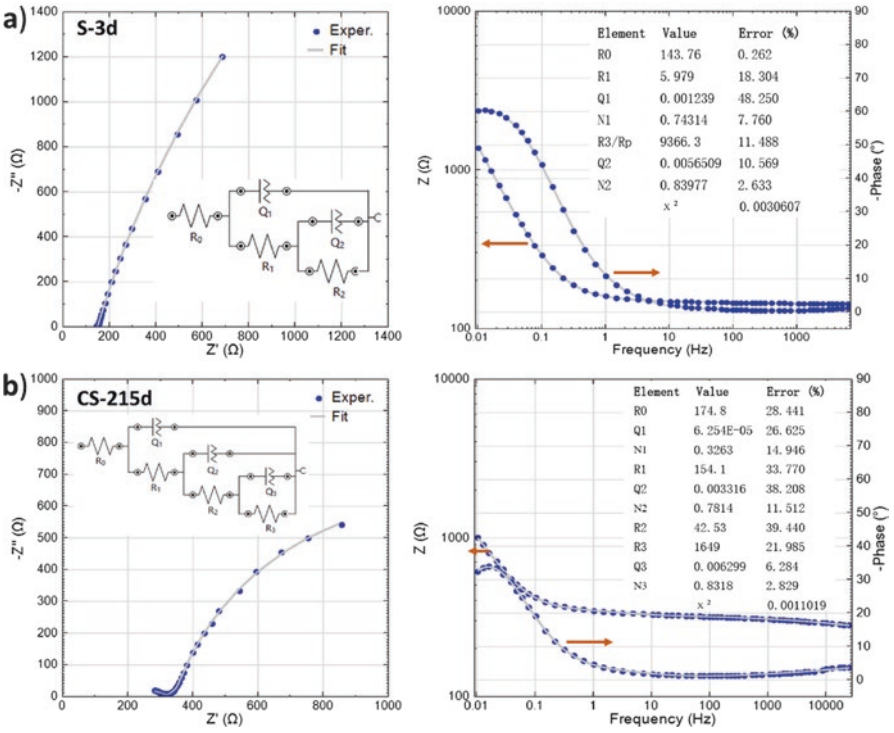

Fig. 5.10 Experimental EIS response and fit for: (**a**) S-3d and (**b**) CS-215d

Q_1) is attributed to the pore network of the mortar matrix, where R_1 and Q_1 are the resistance and pseudo-capacitance of the bulk matrix (the replacement of pure capacitance C with constant phase element Q is a general approach when higher level of heterogeneity is relevant to the system under study [18]). The second time constant for the two-time constant circuit (R_2 and Q_2) deals with the electrochemical reaction (charge transfer process and mass transport process) on the steel surface. The resistance R_2 in this case represents the polarization resistance R_p. In the three-time constant circuit, R_3 and Q_3 correspond to the electrochemical reaction on the steel surface. The first two time constants are attributed to the bulk matrix + electrolyte resistance, including disconnected pore space (R_1 and Q_1), while R_2 and Q_2 represent the resistance and pseudo-capacitance of the connected pore space. A separation between connected and disconnected pore space in specimens C and CS (i.e., additional time constant for the HF domain) is more pronounced and relevant as a result from the influence of the chloride-containing medium on the bulk matrix properties and subsequent alterations in cement hydration and chloride binding mechanisms [22].

The best fit parameters after electrochemical fit and simulation of the relevant system are also included in Fig. 5.10 – inlet in the Bode plots. Detailed presentation

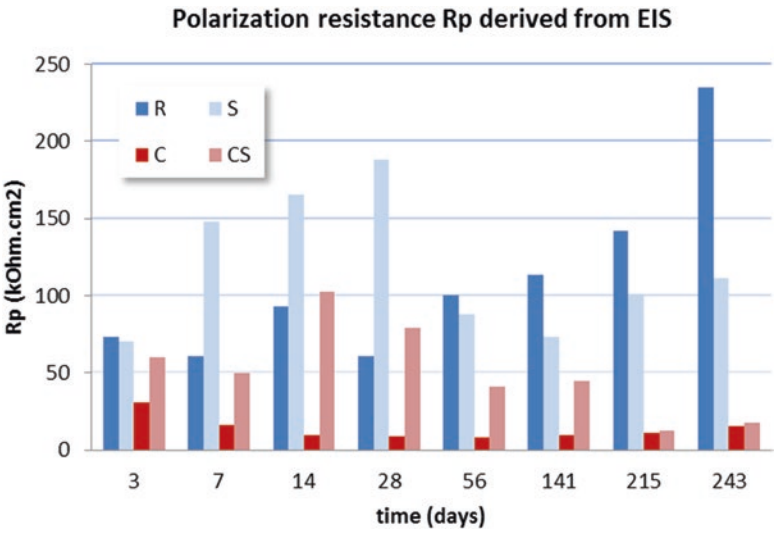

Fig. 5.11 Evolution of polarizations resistance (R_p) for control group (R), stray current group (S), corroding group (C) and corrosion under stray current group (CS). R_p values are as derived from the best fit paramaters from fitting the EIS response, i.e., determined from the evolution of recorded resistance for the last time constant of the employed equivalen circuits

and discussion of all derived parameters is not subject to this work, since the purpose of EIS presentation and discussion was to mainly illustrate the application of EIS to the system under study and correlate results to those from DC electrochemical techniques and derived parameters (Fig. 5.3). Therefore, Fig. 5.11 presents the evolution of global corrosion resistance for all tested specimen groups with time of conditioning (from 3 to 243 days), in terms of polarization resistance values (R_p) as derived from EIS tests.

As can be observed in Fig. 5.11, the R_p values for the control specimens R (non-corroding, water environment) and the specimens S (under stray current in water environment) show a generally increasing trend from 3 to 28 days of treatment. This is in accordance with the expected stabilization of the passive film in the former case (specimens R), although fluctuations in R_p values were recorded through EIS. For the latter case (specimens S), the influence of stray current was expected to potentially exert negative effect on the passive layer formation and stabilization.

However, this was not as observed. On the contrary, the R_p values for specimens S gradually increase in the period of 3–28 days and maintain the highest values among all tested conditions. The reason for this performance for specimens R and S is the already discussed synergetic effect of electrochemically cleaned, i.e., initially active surface and the effects of fresh (non-mature) cement matrix, together with concentration gradients of external environment – cement-based material and steel/cement paste interface. For specimens R all these result in a delay in passive layer formation and stabilization, whereas for specimens S, the current flow induces a positive effect of enhanced cement hydration and consequently favorable

environment for the steel reinforcement. While for specimens S the trend of R_p evolution as derived from EIS is very well in line with the R_p values derived from LPR (Fig. 5.3), i.e., increasing corrosion resistance between 3 and 28 days, this is not entirely the case for specimens R, where R_p values from EIS and LPR significantly differ. This observation supports the hypothesis for the initially more rapid formation and stabilization of the product layer on the steel surface of specimens S, if compared to specimens R for that time period of the test. This results in a higher R_p due to the contribution of a product layer with higher resistance in specimen S, if compared to specimens R, where the derived R_p (from both LPR and EIS) is mainly related to charge transfer resistance.

It should be noted that the absolute values of R_p as derived from both methods are not entirely comparable due to the fact that LRP is a DC and EIS – an AC measurement. Although LPR induces a small DC polarization, EIS applies a 10 mV AC perturbation only. In the case of not yet stable passive (or product) layer on the steel surface, and in view of the range of recorded OCP values (Fig. 5.3), the LPR measurement can result in under- or overestimation of R_p. Therefore, a comparison of trends is always relevant, rather than discussion of absolute values. Additionally, the EIS tests exert minimum or none effect on the forming passive layer on the steel surface and include the resistance of the undisturbed product layer at the time of measurement, in addition to the charge transfer resistance. This gives the global R_p values within EIS tests, which can end up higher if compared to R_p, derived from LPR measurement in these relevant conditions.

From 28 days onwards and until the end of the test of 243 days of conditioning, the already stabilized steel surface and the increased maturity level of the cement-based matrix result in an increasing trend only for the R_p values for specimens R, derived from both EIS (Fig. 5.11) and LPR (Fig. 5.3). In fact, at the end of the test, the R_p values and corrosion resistance, respectively, for specimens R are the highest from all tested cases (as expected). In contrast, the decreasing trend of R_p for specimens S after 28 days and until 243 days already proves the negative effect of stray current on steel passivity, although the corrosion state of specimens S is still superior if compared to the corroding specimens C and CS. In other words, stray current, even in conditions of chloride-free environment, would potentially result in significantly reduced corrosion resistance in the long term.

The R_p values derived from EIS for specimens C and CS (chloride-containing environment) are significantly lower, compared to these for groups R and S, which was as expected. Both corroding groups present more significant fluctuations in R_p values between 3 and 28 days, due to reasons already discussed for groups R and S. Additionally, the combined action of chloride ions and stray current in group CS results in initially higher R_p compared to group C, with a decreasing trend towards the end of the test. The evolution of R_p derived from EIS is in line with that derived from LPR and the responsible phenomena are as already discussed with respect to Fig. 5.3. Additionally, the reason behind similar EIS and LPR response for the corroding groups at all time intervals (which is in contrast to that for the groups S and R for the initial period) is because of the predominance of corrosion initiation and propagation in these two cases, rather than processes related to product layer

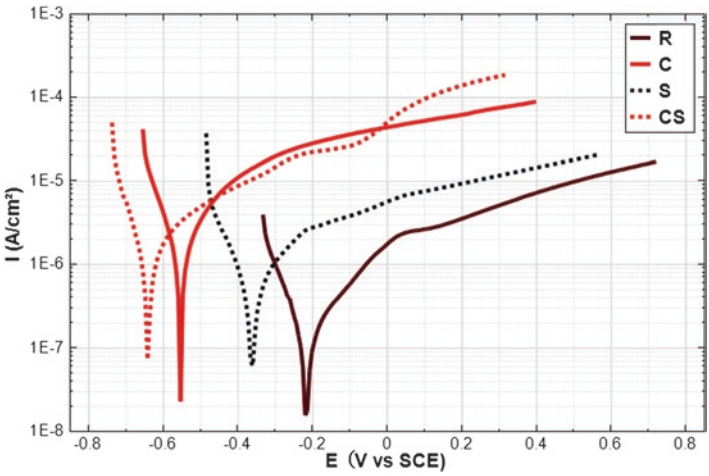

Fig. 5.12 Potentio-dynamic curves for all specimens at 243 days of age

stabilization. Therefore, both techniques result in determination of similarly active state for specimens C and CS.

If the significance of stray current within corrosion initiation and propagation in chloride-containing environment is to be evaluated (specimens C and CS), both EIS and LPR show that a clear evidence for a substantial stray current effect is not present. The corrosion resistance for both C and CS groups was similar at the end of the test. This is most likely denoted to the fact that within the period of 3–28 days, the stray current induced positive effects in view of ion and water migration and enhanced cement hydration – also evident from the response for both C and CS in the high frequency domain of EIS measurements (Fig. 5.9). Therefore, in specimens CS, competing mechanisms were initially involved, and the predominance of chloride-induced corrosion acceleration due to stray current is only relevant on later stages of cement hydration and treatment. These considerations are actually supported by the results from potentio-dynamic polarization, performed at the end of the test – Fig. 5.12.

Figure 5.12 presents the polarization curves for all investigated specimens at 243 days of age. The measurements were performed after 24 h depolarization for the under current regimes (CS and S), i.e., after awaiting for the establishment of a stable OCP of the steel reinforcement. What can be observed is that the most noble potential (approx. -220 mV) and lowest corrosion current were recorded for specimen R – as expected and in line with all other tests. The corrosion potential for specimens S is more cathodic (approx. -380 mV) and the corrosion current is approximately one order higher than that for specimens R. Additionally, larger anodic current within polarization was recorded for specimen S. Here again, stray

current induces corrosion in reinforced cement-based materials and reduces the corrosion resistance, despite the chloride-free environment for specimens S.

The cathodic shift of corrosion potential is more evident for the specimens C and CS, both already more cathodic than −500 mV, Fig. 5.12. Additionally, the corrosion current densities for both C and CS are already significantly higher. These are in line with the, as recorded from all other tests, active state of specimens C and CS. If a comparison is made between specimens C and CS, what can be observed is that, although specimens CS present a more cathodic corrosion potential, the corrosion current is in the same order as that for specimens C. This means that both groups are relatively similar in corrosion activity, as also derived from EIS and LPR in view of similar R_p values at the end of the test. However, the initially higher corrosion resistance in specimens CS (Figs. 5.3 and 5.7) and the potentially positive effect of the stray current in view of ion transport and enhanced cement hydration, hence favorable environment at the steel surface, are well reflected by the behavior of CS with external polarization. As can be observed in Fig. 5.12, the lower anodic currents with external polarization and increase only after the region of around 0 V are denoted to impeded dissolution, i.e., to a more resistive or larger in surface area product layer on the steel surface in CS, if compared to specimen C. This results in initially higher R_p values for specimen CS (as recorded and already discussed), despite the otherwise similarly to C active state.

What can be concluded is that the effect of stray current for both chloride-free (specimens S) and chloride-containing (specimens CS) conditions is predominantly positive in the initial stages of this test and exerts the expected negative influence towards corrosion acceleration after a prolonged treatment and within already a more stable maturity level of the cement-based matrix. This also means that the effect of the cement-based material in reinforced cement-based system is of significant importance and largely determines the electrochemical state of the steel reinforcement.

5.4 Conclusions

In this work, a comparative study was proposed for investigating the different effects of stray current on bulk matrix and the corrosion behavior of embedded steel. Based on the experimental and analytical results, the following conclusions can be drawn:

1. The effect of stray current on concrete bulk matrix properties, together with steel corrosion response, is significantly determined by the external environment, as well as by the level of maturity of the cement-based bulk matrix. Stray current is predominantly positive in the initial stages of this test, but the expected negative influence towards corrosion acceleration was observed after a prolonged treatment, when a stable maturity level of the cement-based matrix was at hand.
2. For chloride-free environment, the effect of the chosen stray current level was not significant, although lower corrosion resistance of the steel rebar was

recorded after longer exposure of 240 days. Positive effects of the stray current were observed in the early stages of the experiment (until 28 days), which were related to enhanced ion and water migration and consequently increased cement hydration and passive film development in the highly alkaline environment of the mortar bulk matrix.

3. In terms of the chloride-contained environment (C and CS groups), active steel surface was detected as expected, due to chloride-induced corrosion initiation in both cases and additional stray current contribution in the case of CS specimens. However, the pronounced effect of the stray current in group CS towards enhanced corrosion was not observed. Based on this, a competitive mechanisms acting in specimens CS can be proposed: on the one hand the stray current has positive effects on bulk matrix properties, similar to specimen S, at early stages. On the other hand, stray current influences chloride ions migration, leading to chloride-induced corrosion and active state, similarly to specimens C.

References

1. Bertolini L, Carsana M, Pedeferri P (2007) Corrosion behaviour of steel in concrete in the presence of stray current. Corros Sci 49(3):1056–1068. doi:10.1016/j.corsci.2006.05.048
2. Metwally IA, Al-Mandhari HM, Gastli A, Al-Bimani A (2008) Stray currents of ESP well casings. Eng Anal Bound Elem 32(1):32–40. doi:10.1016/j.enganabound.2007.06.003
3. Revie RW (2008) Corrosion and corrosion control. Wiley, New York
4. Wang CL, Ma CY, Wang Z (2007) Analysis of stray current in metro DC tractionpower system. Urban Mass Transit 3:51–56
5. Wu M (2011) Progress of the durability of concrete structure of the subway (trans: Hainan University CoCE, Architecture, Guizhou University CoC, Architecture E, Hainan Society of T, Applied M). In: 1st international conference on civil engineering, architecture and building materials, CEABM 2011, .vol 250–253. Haikou. doi:10.4028/www.scientific.net/AMR.250-253.1456
6. Sandrolini L (2013) Analysis of the insulation resistances of a high-speed rail transit system viaduct for the assessment of stray current interference. Part 1: measurement. Electr Power Syst Res 103:241–247. doi:10.1016/j.epsr.2013.04.011
7. Chen Z, Koleva D, Koenders E, van Breugel K (2015) Stray current induced corrosion control in reinforced concrete by addition of carbon fiber and silica fume. MRS Online Proceedings Library 1768:null-null. doi:10.1557/opl.2015.320
8. Radeka R, Zorovic D, Barisin D (1980) Influence of frequency of alternating current on corrosion of steel in seawater. Anti-corros Methods Mater 27(4):13–15+19
9. Kolar V, Hrbac R (2014) Measurement of ground currents leaking from DC electric traction. In: Electric Power Engineering (EPE), Proceedings of the 2014 15th international scientific conference on, 2014. IEEE, pp 613–617
10. Tullmin M (2003–2007). http://www.corrosion-club.com/stfeature1.htm
11. Chang JJ (2003) Bond degradation due to the desalination process. Constr Build Mater 17(4):281–287. doi:10.1016/s0950-0618(02)00113-7
12. Chang JJ, Yeih W, Huang R (1999) Degradation of the bond strength between rebar and concrete due to the impressed cathodic current. J Mar Sci Technol 7(2):89–93
13. Susanto A, Koleva DA, Copuroglu O, van Beek K, van Breugel K (2013) Mechanical, electrical and microstructural properties of cement-based materials in conditions of stray current flow. J Adv Concr Technol 11(3):119–134. doi:10.3151/jact.11.119

14. Standard practice for preparing, cleaning, and evaluating corrosion test specimens (2003) Annual book of ASTM standards (2):17–25
15. Alonso C, Castellote M, Andrade C (2002) Chloride threshold dependence of pitting potential of reinforcements. Electrochim Acta 47(21):3469–3481. doi:10.1016/S0013-4686(02)00283-9
16. Alghamdi SA, Ahmad S (2014) Service life prediction of RC structures based on correlation between electrochemical and gravimetric reinforcement corrosion rates. Cem Concr Compos 47:64–68. doi:10.1016/j.cemconcomp.2013.06.003
17. Sagüés AA, Pech-Canul MA, Shahid Al-Mansur AKM (2002) Corrosion macrocell behavior of reinforcing steel in partially submerged concrete columns. Corros Sci 45(1):7–32. doi:10.1016/S0010-938X(02)00087-2
18. Feliu V, González JA, Feliu S (2004) Algorithm for extracting corrosion parameters from the response of the steel-concrete system to a current pulse. J Electrochem Soc 151(3):B134–B140. doi:10.1149/1.1643737
19. Koleva DA, Van Breugel K, De W, Delft TU, Civil E, Geosciences, Tu Delft DUoT (2007) Corrosion and protection in reinforced concrete: pulse cathodic protection: an improved cost-effective alternative
20. Keddam M, Takenouti H, Nóvoa XR, Andrade C, Alonso C (1997) Impedance measurements on cement paste. Cement Con Res 27(8):1191–1201. doi:http://dx.doi.org/10.1016/S0008-8846(97)00117-8
21. Koleva DA, van Breugel K, de Wit JHW, van Westing E, Boshkov N, Fraaij ALA (2007) Electrochemical behavior, microstructural analysis, and morphological observations in reinforced mortar subjected to chloride ingress. J Electrochem Soc 154(3):E45. doi:10.1149/1.2431318
22. Florea MVA, Brouwers HJH (2012) Chloride binding related to hydration products: part I: ordinary Portland cement. Cem Concr Res 42(2):282–290. doi:10.1016/j.cemconres.2011.09.016. 10.1016/j.conbuildmat.2011.07.045; Brouwers HJH (2011) A hydration model of Portland cement using the work of powers and brownyard, http://www.cement.org, Eindhoven, University of Technology & Portland Cement Association. ISBN: 978-90-6814-184-9
23. Andrade C, Soler L, Novoa XR (1995) Advances in electrochemical impedance measurements in reinforced concrete. Mater Sci Forum 192-194(pt 2):843–856
24. Cui W, Shi Z, Song G, Lin H, Cao CN (1998) Electrochemical study on the reinforced concrete during curing. Corros Sci Prot Technol 10(4):201–207
25. Wenger F, Galland J (1990) Analysis of local corrosion of large metallic structures or reinforced concrete structures by electrochemical impedance spectroscopy (EIS). Electrochim Acta 35(10):1573–1578. doi:10.1016/0013-4686(90)80012-D